

Clothoid-based Lane Change Trajectory Computation for Self-Driving Vehicles

¹Ardam Haseeb Mohammed Ali Kahya and ²Klaus Werner Schmidt

¹Department of Electronic and Communication Engineering, Çankaya University, Ankara, Turkey

²Department of Mechatronics Engineering, Çankaya University, Ankara, Turkey
e-mail: ardamkahi73@yahoo.com, schmidt@cankaya.edu.tr

Abstract: The subject of this paper is the efficient computation of lane change trajectories for self-driving vehicles. The paper first identifies that a certain type of clothoid-based *bi-elementary paths* can be used to represent lane change trajectories for vehicles. It is further highlighted that the curvature of such trajectories must be adjusted to the driving situation in order to obtain feasible lane change trajectories. Accordingly, the paper establishes an analytical relation between the maximum admissible curvature of the lane change trajectory and the velocity profile during a lane change. Using this relation, the paper proposes an efficient Newton iteration for computing the parameters of bi-elementary paths for lane changes. The resulting lane change trajectories are as short as possible, while meeting the constraint on the maximum curvature. Simulation experiments for various driving situations show that the computed bi-elementary paths can be computed efficiently and constitute suitable lane change trajectories.

Keywords: Autonomous vehicles, lane changes, clothoid trajectories.

1. Introduction

Today, the need for a more efficient and smarter usage of the available transportation infrastructure leads to the emergence of *Intelligent Transportation Systems (ITS)*. ITS deployments aim at increasing the traffic throughput and safety, reducing the total travel time and traffic congestion using novel achievements of communication and control technologies [30, 29, 28, 24].

As an important application of ITS, the development of self-driving vehicles (SDVs) gains increasing interest in the recent years. It is expected that SDVs will be available in the near future [2] and it is predicted by IEEE that SDVs will constitute 75 % of cars by 2040 [1]. The usage of SDVs requires the development of advanced methods for controlling the longitudinal and lateral vehicle behavior. In particular, it is required to design vehicle trajectories for different vehicle maneuvers. Hereby, trajectories are considered suitable if they can be easily computed and applied in real-time vehicle applications, while ensuring driving comfort and safety.

The main subject of this paper is the fast computation of trajectories for lane changes of SDVs. To this end, this paper suggests utilizing a certain type of bi-elementary paths for representing

lane change trajectories. Bi-elementary paths are based on clothoid curves and are found suitable for lane change computations in the recent literature [11]. As the first contribution, this paper develops an efficient method for computing the parameters of such bi-elementary path based on a Newton iteration. It is proved that the proposed Newton iteration always converges to a unique solution, whereby fast convergence is observed from computational experiments. As the second contribution of this paper, it is argued that the parameters of bi-elementary paths for lane changes have to be chosen carefully depending on the driving situation. To this end, this paper determines an analytical bound on the admissible path curvature depending on the maximum velocity profile of a vehicle during a lane change. Using this bound, this paper proposes a computational procedure for selecting the parameters of bi-elementary paths that are suitable for lane change trajectories. This parameter selection can be efficiently carried out in real-time based on the current vehicle velocity and a bound on the admissible acceleration. Using the proposed procedure, it is possible to uniquely determine the shortest bi-elementary path that fulfills the imposed curvature constraint depending on the driving situation. Simulation experiments with a nonlinear vehicle model show that the proposed method determines suitable lane change trajectories.

In the existing literature, the generation of lane change trajectories is mostly studied in the context of model predictive control (MPC) or optimal control. [33] used MPC to formulate constraints for finding a lane change trajectory and suitable input signals while avoiding collisions. A disadvantage of MPC is that trajectories are not known in advance but evolves based on the computed lane change steering maneuver. Optimal control is used in [8, 25, 16, 31]. [8] presents an optimal-control based method for quantifying the maneuverability of actively controlled passenger vehicles during emergency highway-speed situations. Necessary conditions for optimality and optimal control laws are found for different cases including rear steering. [25] provide optimal control-based strategies to explore the dynamic capabilities of a single-track car model with tire models and longitudinal load transfer. That paper explores the system dynamics by using nonlinear optimal control techniques to compute aggressive car trajectories. An optimal path-planning method is proposed for self-driving ground vehicles in case of overtaking a moving obstacle in [16]. The trajectory generation problem faced by a self-driving vehicle in moving traffic is investigated in [31]. A semi-reactive planning strategy that realizes long-term maneuvers and ensures short-term collision avoidance is proposed. Although the cited methods determine feasible Lane change trajectories, their main disadvantage is that the trajectories are computed offline when using optimal control. In particular, the required computation times are not suitable for an evaluation in real-time. The research on the computation of lane change trajectories without using optimization methods is limited. An incremental trajectory planner based on rapidly-exploring random trees and a dynamic vehicle model is proposed in [23]. A lane change model for self-driving vehicles was presented in [6]. In this study the emphasis was made on generating a safe path based

on a piecewise Bezier curve. Moreover, the work in [11] analyzes the suitability lane change trajectories based on bi-elementary paths. Different from the existing work, this paper develops a computational procedure for determining suitable parameters for short lane change trajectories depending on the driving situation in real-time.

The remainder of this paper is organized as follows. Section 2 motivates the lane change trajectory computation for self-driving vehicles and formulates the problem studied in this paper. The usage of bi-elementary paths for lane changes and the proposed parameter computation method are discussed in Section 3. In Section 4, the proposed trajectory computation method is validated by simulation experiments. Section 5 gives conclusions and outlines directions for future work.

2. Motivation and Problem Statement

This section motivates the study of trajectory generation for lane changes and states the research topics considered in this paper. Section 2.1 describes basic properties of lane change maneuvers and Section 2.2 introduces bi-elementary paths as a suitable trajectory representation. The main problem considered in this paper is outlined in Section 2.3.

2.1. Background on Lane Change Trajectories

Lane changing is the process, where a vehicle moves from its current lane to an adjacent lane as depicted in Fig. 1.

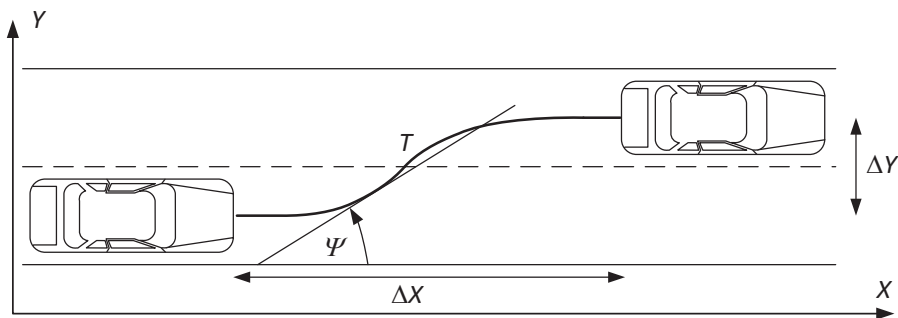


FIGURE 1. Basic lane change maneuver.

A lane change is carried out following a certain trajectory T in the coordinate plane (X - Y -plane). Hereby, the change in the Y -position is given by the lane width ΔY , whereas the change in the X -position and the orientation angle Ψ during the lane change determine the particular shape of T . In principle, a trajectory T with a small value of ΔX requires a fast change of the orientation angle Ψ and is hence difficult to follow when vehicles travel at high velocities or perform acceleration maneuvers. In turn, trajectories T with large values of ΔX permit small variations of Ψ and are

suitable for fast vehicles. The disadvantage of such trajectories is given by the fact that vehicles simultaneously occupy two lanes of a larger segment of the road, leading to an inefficient use of the road infrastructure. Accordingly, it is highly relevant to adjust lane change trajectories T depending on the velocity/acceleration profile of vehicles.

When considering self-driving vehicles, lane change trajectories have to be computed in real-time and lane changes have to be carried out autonomously. In this paper, we assume that a basic control architecture for self-driving vehicles as in Fig. 2 is available.

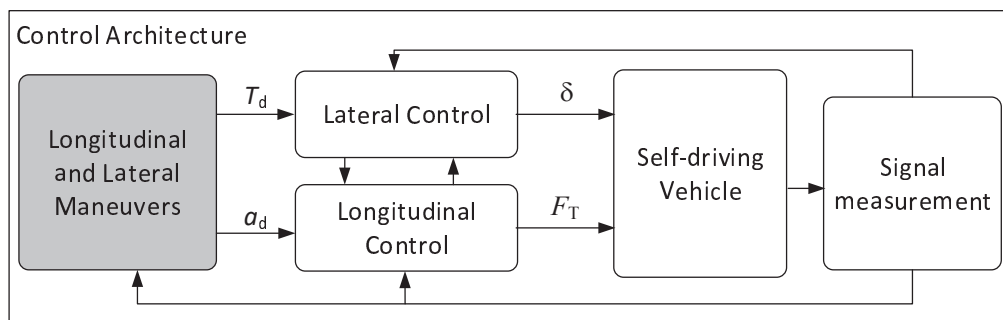


FIGURE 2. Control architecture for self-driving vehicles.

In such architecture, the motion of the self-driving vehicle is controlled by the steering angle δ and the traction force F_T . Desired maneuvers for longitudinal and lateral vehicle maneuvers are computed in real-time and the related reference signals are fed to the respective controllers. The longitudinal controller provides the traction force F_T depending on the desired acceleration signal a_d and the lateral controller determines the required steering angle δ based on the desired vehicle trajectory T_d . Note that both the maneuver generation and the control algorithms depend on signal measurements from the vehicle.

Assuming a control architecture as in Fig. 2, the focus of this paper is on the generation of suitable lane change trajectories T_d depending on the velocity/acceleration profile of vehicles. Specifically, it is desired to employ an analytical representation of lane change trajectories that can be followed by self-driving vehicles, which can be parametrized depending on longitudinal vehicle maneuvers and can be evaluated in real-time.

2.2. Bi-Elementary Paths for Lane Changes

The recent literature indicates that trajectories based on clothoid curves can be used to represent lane change trajectories [27, 13, 11]. The work in this paper is based on *bi-elementary paths* as a special type of clothoid curves.

In general, a bi-elementary path as considered in this paper is shaped as shown in Fig. 3.

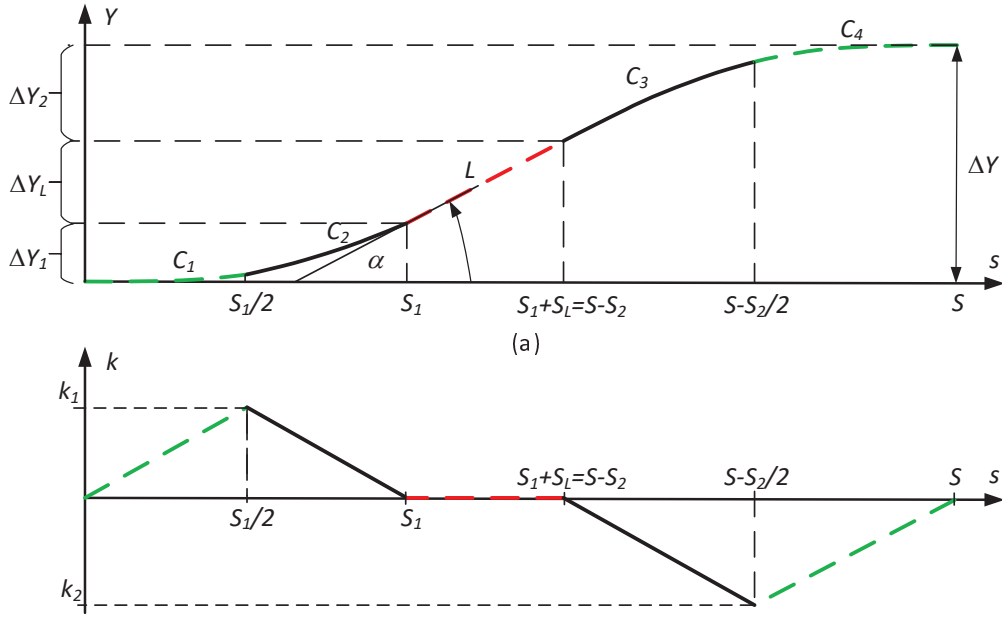


FIGURE 3. Components of a bi-elementary path.

It consists of 5 segments C_1, C_2, L, C_3, C_4 that are defined in terms of the arc-length parameter s . Precisely, s denotes the traveled distance when following the bi-elementary path and S is the total length of the path. The segments C_1, \dots, C_4 are *clothoid curves*, whereas L is a straight *line segment*. During the clothoid curves, the curvature k of the bi-elementary path changes linearly with the arc-length, whereas the curvature is zero during the line segment L . We next formalize the description of a bi-elementary path as a basis for the main results of this paper. The formalization is based on the previous literature in [20, 7, 17, 18, 14, 11].

Since bi-elementary paths are based on clothoid curves, we first provide a formal definition of clothoids. Clothoids are considered as suitable curves for vehicle trajectories since they enable a smooth change of the trajectory curvature [4, 11]. The curvature of a clothoid is defined as

$$k(s) = k_i + \sigma s \quad (1)$$

with the initial curvature k_i and a constant σ that characterizes the change of curvature. Then, the evolution of a clothoid C with arc length S_C in the coordinates X, Y, Ψ is evaluated depending on the arc length parameter s :

$$\Psi(s) = \int_0^s k(z) dz + \Psi_i \quad (2)$$

$$X(s) = \int_0^s \cos(\Psi(z)) dz + X_i \quad (3)$$

$$Y(s) = \int_0^s \sin(\Psi(z)) dz + Y_i \quad (4)$$

Here, Ψ_i, X_i and Y_i represent the initial values for the orientation angle, X -position and Y -position, respectively. In the sequel, we employ the following notation for clothoids. The initial point is written as $P_i = \begin{bmatrix} X_i \\ Y_i \end{bmatrix}$, the initial curvature is $k_i = k(0)$ and the final curvature is $k_f = k(S_C)$. We write

$$C = \mathcal{C}(P_i, \Psi_i, k_i, k_f, S_C) \tag{5}$$

for a clothoid with starting point P_i , initial orientation angle Ψ_i , initial curvature k_i , final curvature k_f and arc length S_C . We note that a clothoid is uniquely characterized by these parameters since the curvature is directly given by

$$k(s) = k_i + \sigma s = k_i + \frac{(k_f - k_i)}{S_C} s. \tag{6}$$

For a given clothoid $C = \mathcal{C}(P_i, \Psi_i, k_i, k_f, S_C)$, we introduce the notation $P_i(C) = P_i$, $\Psi_i(C) = \Psi_i$, $k_i(C) = k_i$, $k_f(C) = k_f$ and $S(C) = S_C$. In addition, the change in orientation angle is computed as

$$\Delta\Psi(C) = \frac{(k_f + k_i) S_C}{2} \tag{7}$$

and the final tangent angle is

$$\Psi_f(C) = \Psi_i + \Delta\Psi(C). \tag{8}$$

We further write $Y_f(C)$ for the final Y -position of C .

The clothoid curves C_1 and C_2 of a bi-elementary path as in Fig. 3 form a so-called *elementary path*. It holds for the arc-length that $S_{C_1} = S_{C_2} = S_1/2$ and the curvatures fulfill

$$k_{C_1}(s) = \frac{2k_1}{S_1} s \text{ (for } s \in [0, S_1/2]) \quad \text{and} \quad k_{C_2}(s) = \frac{2k_1}{S_1} (S_1 - s) \text{ (for } s \in (S_1/2, S_1]). \tag{9}$$

In addition, the initial point of C_2 is the final point of C_1 , the initial angle of C_2 is the final angle of C_1 and the initial curvature of C_2 is the final curvature k_1 of C_1 . Writing P_i for the initial point of C_1 and Ψ_i for the initial angle of C_1 , such elementary path is defined by the two clothoid curves

$$C_1 = \mathcal{C}(P_i, \Psi_i, 0, k_1, S_1/2) \tag{10}$$

$$C_2 = \mathcal{C}(P_f(C_1), \Psi_f(C_1), k_1, 0, S_1/2) \tag{11}$$

and is written as

$$\mathcal{E}(P_i, \Psi_i, k_1, S_1) \tag{12}$$

in the remainder of this paper. Noting that $P_i = 0$ and $\Psi_i = 0$ for the elementary path given by C_1 and C_2 , this elementary path is precisely described by

$$E_1 = \mathcal{E}(0, 0, k_1, S_1). \tag{13}$$

The second part of the bi-elementary path in Fig. 3 is a straight line segment L that is defined by its arc-length S_L , its initial point $P_f(E_1)$ and its orientation angle $\alpha = \Psi_f(E_1)$. Hence, this line

segment is written as

$$L = \mathcal{L}(P_f(E_1), \Psi_f(E_1), S_L). \quad (14)$$

It can be further observed that the curves C_3 and C_4 in Fig. 3 form an elementary path that is described by

$$E_2 = \mathcal{E}(P_f(L), \alpha, k_2, S_2). \quad (15)$$

In order to ensure that the tangent orientation $\theta_f(E_2)$ at the end of the bi-elementary path is zero and respecting (7), it must hold that

$$\Psi_f(E_2) = \frac{k_2 S_2}{2} = -\Psi_f(E_1) = -\frac{k_1 S_1}{2} = -\alpha.$$

That is,

$$k_2 = -\frac{k_1 S_1}{S_2}. \quad (16)$$

2.3. Problem Formulation

Together, a bi-elementary path consists of the concatenated segments E_1 in (13), L in (14) and E_2 in (15) and is defined by its maximum curvature k_1 and the shares S_1 , S_L , S_2 of the different segments in the total arc-length S .

There are two main problems to be solved regarding the selection of these parameters when computing lane change trajectories for self-driving vehicles.

1. It needs to be ensured by a correct choice of k_1 , S_1 , S_L and S_2 that the change of the Y -position of a bi-elementary path equals the actual lane width. Since the position of a clothoid path cannot be evaluated analytically [4, 13], efficient numerical methods are required to achieve this task.
2. The selection of each parameter affects the shape of the bi-elementary path and hence the drivability of the corresponding lane change trajectory. That is, different parameters must be chosen depending on the velocity profile and/or acceleration profile of a vehicle.

In Section 3, this paper develops novel computational methods in order to address the stated requirements. Furthermore, a simulation study in Section 4 validates the suitability of the developed methods.

3. Computation of Lane Change Trajectories

This section constitutes the main contribution of this paper. First, Section 3.1 summarizes several properties of bi-elementary paths that are required for the efficient parameter computation in Section 3.2. A novel method for the parameter selection of bi-elementary paths depending on the driving situation is proposed in Section 3.3 and illustrated by example trajectory computations in Section 3.4.

3.1. Basic Properties of Bi-elementary Paths

Using the same notation as in Section 2.2, several facts about elementary paths are derived from [11]. Using the change in orientation angle

$$\alpha = \frac{k_1 S_1}{2}$$

from (16) and the function

$$D(\alpha) = 2 \int_0^{0.5} \cos(2\alpha(-z^2 + z)) dz, \quad (17)$$

the change in the Y -position of a generic bi-elementary path in Fig. 3 can be evaluated as

$$\Delta Y = \Delta Y_1 + \Delta Y_L + \Delta Y_2 = S_1 D(\alpha) \sin(\alpha/2) + S_L \sin(\alpha) + S_2 D(\alpha) \sin(\alpha/2). \quad (18)$$

We next suggest two modifications of the computation in (18). First, it has to be respected that it is not possible to evaluate (17) analytically. Instead, we compute $D(\alpha)$ for the relevant range of values for α and use an approximation of the resulting curve. From the practical perspective, the orientation angle of a lane changes stays well below a value of $\alpha < \pi/4$. Hence, an interval of $\alpha \in [-\pi/4, \pi/4]$ is used for the approximation. Noting that $D(\alpha) = D(-\alpha)$, it is hence, sufficient to evaluate $D(\alpha)$ in the interval $[0, \pi/4]$. The resulting function evaluation is shown in Fig. 4 together with a tight polynomial approximation of degree 3. In the sequel, we employ this approximation

$$\hat{D}(\alpha) = p_0 + p_1 \alpha + p_2 \alpha^2 + p_3 \alpha^3 \quad (19)$$

with the parameters $p_0 = 1$, $p_1 = 1.34 \cdot 10^{-4}$, $p_2 = -6.75 \cdot 10^{-2}$ and $p_3 = 1.64 \cdot 10^{-3}$. The approximation is chosen such that the residual norm is below 10^{-5} .

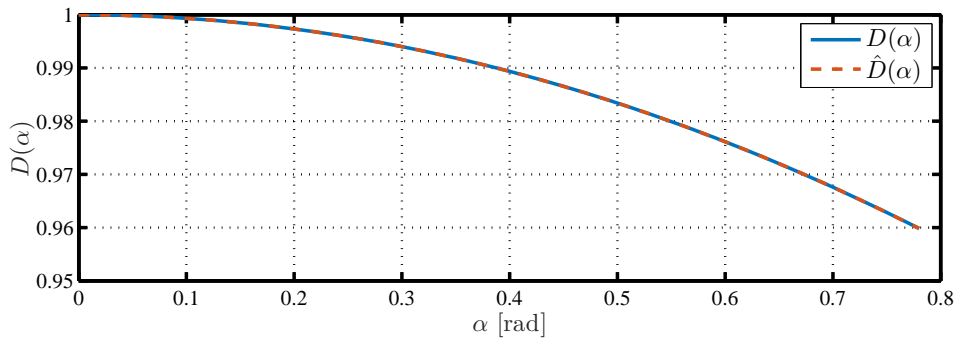


FIGURE 4. Approximation of $D(\alpha)$

In addition, it will be more convenient to consider a different parametrization of a bi-elementary path based on the share of each segment in the overall arc-length S . To this end, we introduce the

parameters $\lambda \in (0, 1)$ and $\gamma \in (0, 1]$ and define

$$S_1 + S_2 = \gamma S \quad (20)$$

$$S_L = (1 - \gamma)S \quad (21)$$

$$S_1 = \lambda \gamma S \quad (22)$$

$$S_2 = (1 - \lambda) \gamma S. \quad (23)$$

That is, γ represents the length of the elementary paths in relation to the overall arc length S . A large value of γ (and hence small value of $1 - \gamma$) implies a short straight line segment L . The ratio of the arc-lengths of the elementary paths E_1 and E_2 is given by λ . If $\lambda > 0.5$, it holds that E_1 is longer than E_2 and vice versa. Using these shape parameters λ and γ , a bi-elementary path can be written as

$$\mathcal{B}(S, k_1, \lambda, \gamma). \quad (24)$$

Using $\hat{D}(\alpha)$ in (19), the overall change in the Y -position is approximated as

$$\begin{aligned} \Delta \hat{Y} &= S_1 \hat{D}(\alpha) \sin(\alpha/2) + S_L \sin(\alpha) + S_2 \hat{D}(\alpha) \sin(\alpha/2) \\ &= \lambda \gamma S \hat{D}(\alpha) \sin(\alpha/2) + (1 - \gamma) S \sin(\alpha) + (1 - \lambda) \gamma \hat{D}(\alpha) \sin(\alpha/2) \\ &= S (\gamma \hat{D}(\alpha) \sin(\alpha/2) + (1 - \gamma) \sin(\alpha)). \end{aligned} \quad (25)$$

For illustration, Fig. 5 and 6 show bi-elementary paths with the arc-length $S = 100$ and curvature $k_1 = 0.005$ for different values of λ and γ . The variation of λ in Fig. 5 indicates that choosing a larger value of λ (a longer first elementary path E_1) also leads to a larger change in the Y -position. The same effect is observed for a larger value of γ (a shorter straight line segment L) in Fig. 6.

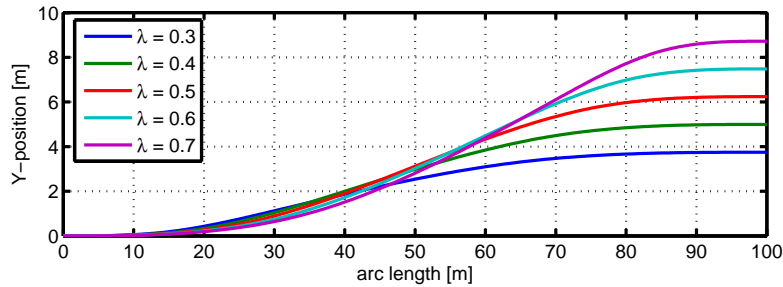


FIGURE 5. $\mathcal{B}(S, k_1, \lambda, \gamma)$ for $S = 100$, $k_1 = 0.005$, $\gamma = 1$ and different values of λ .

3.2. Parameter Computations

When computing lane change trajectories for self-driving vehicles based on bi-elementary paths, it is required to determine the relevant parameters S , λ , γ , ΔY , k_1 and α . According to the previous

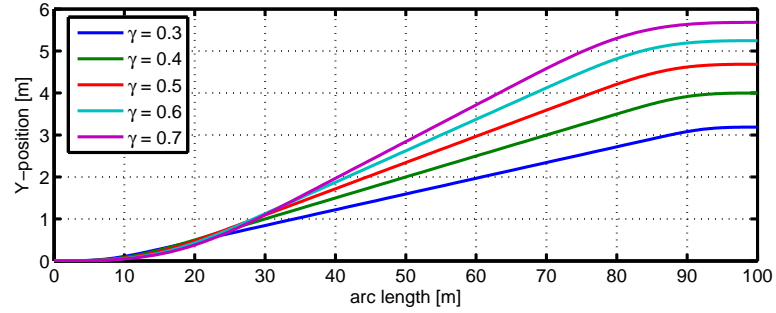


FIGURE 6. $\mathcal{B}(S, k_1, \lambda, \gamma)$ for $S = 100$, $k_1 = 0.005$, $\lambda = 0.5$ and different values of γ .

discussion, these 6 parameters are related by the following equations:

$$\Delta \hat{Y} = S (\gamma \hat{D}(\alpha) \sin(\alpha/2) + (1 - \gamma) \sin(\alpha)) \quad (26)$$

$$\alpha = \frac{\lambda \gamma S k_1}{2} \quad (27)$$

That is, it is only required to assign four of these parameters. The remaining parameters can then be computed from (26) and (27).

Regarding the choice of the fixed parameters, we consider a special case that is most relevant in practice and that is the basis for the novel parameter selection method in Section 3.3. In this case, the change in the Y -position ΔY , the shape parameters λ and γ and the curvature parameter k_1 are known. Since $|k_1|$ denotes the maximum curvature of the first elementary path E_1 and $|k_2| = \frac{\lambda k_1}{1 - \lambda}$ denotes the maximum curvature of the second elementary path E_2 , the choice of k_1 determines the maximum curvature encountered along the bi-elementary path. From the practical perspective, the drivability of a bi-elementary path is directly related to the values of k_1 and k_2 as will be further elaborated in Section 3.3. Intuitively, it holds that trajectories with a large curvature can only be followed at small velocities. That is, specifying the value of k_1 for a lane change is directly related to the admissible velocity during a lane change.

In the described case, ΔY , λ , γ and k_1 are given, and it is required to determine α and S . We know from (26) and (27) that

$$\alpha = \frac{\gamma \lambda S k_1}{2} \Rightarrow S = \frac{2 \alpha}{\lambda \gamma k_1}.$$

This can be substituted in (26) and we get

$$\Delta Y \approx \Delta \hat{Y} = \frac{2 \alpha}{\lambda \gamma k_1} (\gamma \hat{D}(\alpha) \sin(\alpha/2) + (1 - \gamma) \sin(\alpha)).$$

This gives a nonlinear equation for α :

$$f_1(\alpha) = 2 \alpha (\gamma \hat{D}(\alpha) \sin(\alpha/2) + (1 - \gamma) \sin(\alpha)) - \lambda \gamma k_1 \Delta Y = 0. \quad (28)$$

It is desired to obtain a fast solution of the nonlinear equations in (28) in order to evaluate bi-elementary paths for lane changes in real-time. We next show that the Newton method is suitable for this purpose and even provides a unique solution. To this end, we first briefly describe the Newton method. Consider the equation $f(z) = 0$, where $f(z)$ is a nonlinear function. Using an initial value z_0 and the first derivative $f'(z) = \frac{\partial f(z)}{\partial z}$ of $f(z)$, the Newton iteration proceeds as follows

$$z_{i+1} = -\frac{f(z_i)}{f'(z_i)} + z_i, \quad i = 0, 1, \dots \quad (29)$$

The iteration terminates if $|f(z_{i+1})| < \varepsilon$, where ε is a small tolerance value. We next show in Theorem 1 that the Newton iteration converges to a unique solution when solving (28).

Theorem 1. Consider that $\alpha \in [0, \pi/4]$, $0 \leq \gamma \leq 1$, $0 \leq \lambda \cdot k_1 \leq 0.05$ and $0 < \Delta Y \leq 10$. Then, the nonlinear equation in (28) has a unique solution α^* that can be computed by the Newton iteration in (29) with the initial value $\alpha_0 = \pi/4$.

The proof of Theorem 1 is provided in Appendix A. In words, Theorem 1 confirms that the Newton iteration with the function $f_1(\alpha)$ in (28) converges to the unique solution α^* . Applying $S^* = \frac{2\alpha^*}{\lambda \gamma k_1}$, this leads to a lane change with width ΔY using the bi-elementary path $\mathcal{B}(S^*, k_1, \lambda, \gamma)$. When applying Theorem 1, the defined bounds for λ , γ , k_1 and ΔY need to be justified. By (21) to (23), it is clear that $0 \leq \lambda, \gamma \leq 1$. In addition, it holds that the curvature parameter k_1 represents the inverse of the road radius. Considering that the smallest possible radius for a vehicle is given by the turning circle radius R_T , it must hold that $k_1 \leq 1/R_T$ and $|k_2| = \frac{\lambda k_1}{1-\lambda} \leq 1/R_T$. That is,

$$\frac{\lambda k_1}{1-\lambda} \leq 1/R_T \Rightarrow \lambda (k_1 + 1/R_T) < 1/R_T \Rightarrow \lambda < \frac{1/R_T}{k_1 + 1/R_T} \Rightarrow \lambda k_1 < \frac{1/R_T k_1}{k_1 + 1/R_T}$$

Considering that k_1 is bounded by $1/R_T$, the bound for λk_1 is given by

$$\lambda k_1 < \frac{1/R_T \cdot 1/R_T}{1/R_T + 1/R_T} = \frac{1}{2R_T}. \quad (30)$$

Applying the fact that the turning radius of series vehicles is usually not below 10m, it can hence be assumed that $\lambda k_1 \leq 0.05$. In addition, ΔY represents the lane width for a lane change. When performing a single lane change, the lane width is usually assumed as $\Delta Y = 3.7$ m. Also allowing for multiple or wider lane changes, we consider a bound of $\Delta Y \leq 10$.

For illustration, we next provide several examples for bi-elementary paths that were computed using the Newton iteration with $\varepsilon = 10^{-8}$ as described above with $\Delta Y = 3.7$ and different values for k_1, λ, γ . Note that the termination criterion corresponds to a deviation of $1 \mu\text{m}$ from the desired lane change width $\Delta Y = 3.7$ m, which is more than sufficient in practice. Fig. 7 shows the case where k_1 is varied for given values of $\lambda = 0.5$ and $\gamma = 1$. It can be seen that a larger curvature leads to trajectories with a shorter arc-length.

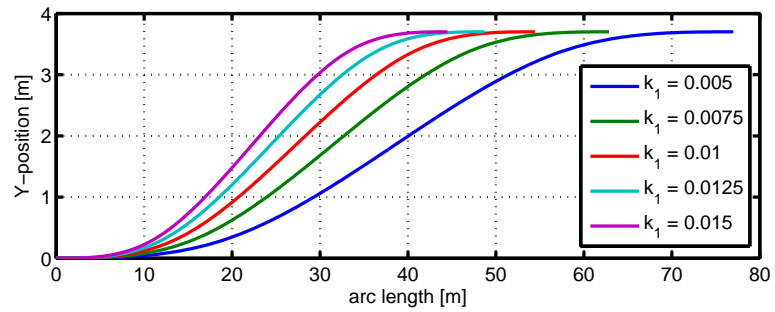


FIGURE 7. $\mathcal{B}(S, k_1, \lambda, \gamma)$ for $\Delta Y = 3.7$, $\lambda = 0.5$, $\gamma = 1$ and different k_1 .

A similar effect is observed when increasing the shape parameters λ and γ in Fig. 5 and 6, respectively. In all computational experiments, the Netwon method converged within at most 7 iterations despite the very tight termination condition.

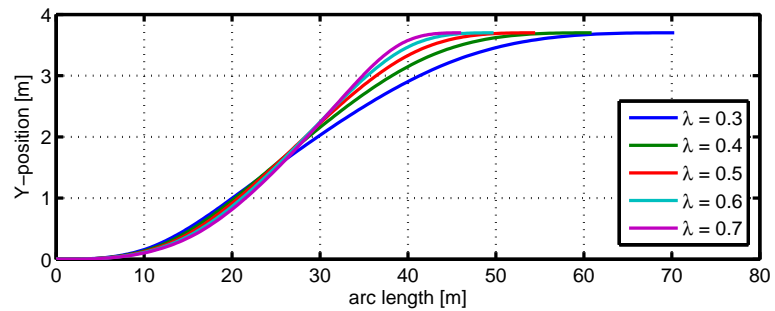


FIGURE 8. $\mathcal{B}(S, k_1, \lambda, \gamma)$ for $\Delta Y = 3.7$, $k_1 = 0.01$, $\gamma = 1$ and different λ .

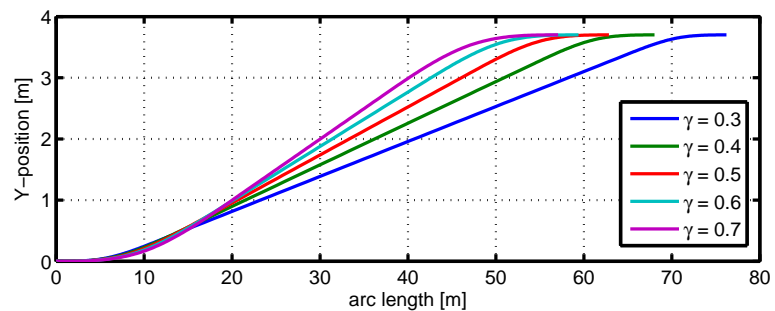


FIGURE 9. $\mathcal{B}(S, k_1, \lambda, \gamma)$ for $\Delta Y = 3.7$, $k_1 = 0.01$, $\lambda = 0.5$ and different γ .

3.3. Parameter Selection Method

The method presented in the previous section enables the efficient computation of bi-elementary paths assuming that the relevant parameters such as k_1 , λ and γ are already given. The remaining

question is the selection of these parameters depending on the driving situation. Qualitatively, it holds that small curvature values (and hence long trajectories) should be chosen at large speeds and/or accelerations, whereas large curvature values (short trajectories) can be tolerated at small velocities. In the sequel, we develop a method for selecting the relevant parameters based on a characterization of the maximum possible curvature for a given velocity/acceleration profile.

To this end, we assume that the *entry velocity* of a lane change is v_0 and the maximum acceleration during a lane change is a_{\max} . In practice, the entry velocity is the current vehicle velocity when initiating a lane change and hence available. In addition, a_{\max} is determined by the limits for comfortable driving which are in the order of $a_{\max} = 2 \text{ m/sec}^2$ [32, 9, 19]. Using v_0 and a_{\max} , the maximum velocity profile during a lane change is given by

$$v(t) = v_0 + a_{\max} t \quad (31)$$

and the corresponding arc-length is computed as

$$s(t) = v_0 t + \frac{1}{2} a_{\max} t^2. \quad (32)$$

Since bi-elementary paths are formulated depending on the arc-length parameter s , we next write the maximum velocity profile in terms of the arc-length as

$$t(s) = \frac{1}{a_{\max}} (-v_0 + \sqrt{v_0^2 + 2a_{\max} s}), \quad (33)$$

$$v_{\max}(s) = v_0 + a_{\max} t(s) = v_0 - v_0 + \sqrt{v_0^2 + 2a_{\max} s} = \sqrt{v_0^2 + 2a_{\max} s}. \quad (34)$$

It is now possible to establish a relation between the maximum velocity profile in (34) and the maximum feasible curvature based on the well-established friction circle [21]. Assuming a point mass vehicle model as in [11], it must hold that

$$a_{\text{long}}^2 + a_{\text{lat}}^2 \leq \mu^2 g^2, \quad (35)$$

whereby, a_{long} is the longitudinal vehicle acceleration, a_{lat} is the lateral vehicle acceleration, μ is the friction coefficient of the road and g is the gravity constant. Moreover, the lateral acceleration on a curved road with radius R and curvature $k = 1/R$ depends on the longitudinal velocity $v(s)$ via

$$a_{\text{lat}}(s) = \frac{v(s)^2}{R} = v(s)^2 \cdot k. \quad (36)$$

Respecting that $a_{\text{long}} \leq a_{\max}$, the maximum curvature profile is derived as

$$k_{\max}(s) = \frac{\sqrt{\mu^2 \cdot g^2 - a_{\max}^2}}{v_{\max}^2(s)} = \frac{\sqrt{\mu^2 \cdot g^2 - a_{\max}^2}}{v_0^2 + 2a_{\max} s} \quad (37)$$

In words, any lane change trajectory with a curvature, whose absolute value at each arc-length s remains below $k_{\max}(s)$ can be taken by vehicles that enter the lane change with velocity v_0 and

whose acceleration is bounded by a_{\max} . Moreover, in view of the previous discussion on lane change trajectories in Section 2.1, it is desired to find a shortest possible bi-elementary path with a curvature that is bounded by $k_{\max}(s)$.

Consider a generic bi-elementary path $\mathcal{B}(S, k_1, \lambda, \gamma)$. According to Fig. 3, the maximum curvature is reached at $s = \lambda \gamma S/2$ with a curvature value k_1 and at $s = S - (1 - \lambda) \gamma S/2$ with a curvature value $k_2 = -\lambda/(1 - \lambda) k_1$. In order to determine a bi-elementary path with the shortest arc-length (and hence largest curvature), it is required to achieve

$$k_1 = k_{\max}(\lambda \gamma S/2) \text{ and } k_2 = -\lambda/(1 - \lambda) k_1 = -k_{\max}(S - (1 - \lambda) \gamma S/2). \tag{38}$$

Substituting (38) into (37), it follows that

$$k_{\max}(s_2) = \frac{\lambda}{1 - \lambda} k_{\max}(s_1) \tag{39}$$

$$\Rightarrow \frac{\sqrt{\mu^2 \cdot g^2 - a_{\max}^2}}{v_0^2 + 2a(S - (1 - \lambda) \gamma S/2)} = \frac{\lambda}{1 - \lambda} \frac{\sqrt{\mu^2 \cdot g^2 - a_{\max}^2}}{v_0^2 + 2a \lambda \gamma S/2} \tag{40}$$

This equation can be solved for λ and the corresponding value of k_1 follows from (38).

$$\lambda_{\max} = f_{\lambda}(S) = \frac{(S a_{\max} - \sqrt{S^2 a_{\max}^2 \gamma^2 - 2 S^2 a_{\max}^2 \gamma + S^2 a_{\max}^2 + 2 S a_{\max} v_0^2 + v_0^4 + v_0^2 - S a_{\max} \gamma})}{2 S a_{\max} \gamma} \tag{41}$$

$$k_{1,\max} = f_{k_1}(S, \lambda) = \frac{\sqrt{g^2 \cdot \mu^2 - a_{\max}^2}}{v_0^2 + S \cdot a_{\max} \cdot \gamma \cdot \lambda} \tag{42}$$

That is, (41) and (42) must be fulfilled in order to achieve the maximum feasible curvature. In addition, (28) must be ensured to obtain the desired lane width ΔY . In the sequel, we reformulate (28) in terms of the arc-length S by substituting $\alpha = \frac{\lambda \gamma k_1 S}{2}$. Accordingly, it must hold that

$$f_S(S, k_1, \lambda, \gamma) = S \left(\gamma \hat{D}\left(\frac{\lambda \gamma k_1 S}{2}\right) \sin\left(\frac{\lambda \gamma k_1 S}{4}\right) + (1 - \gamma) \sin\left(\frac{\lambda \gamma k_1 S}{2}\right) \right) - \Delta Y = 0. \tag{43}$$

Substituting (41) and (42) into (43), we must solve

$$f_S(S, f_{k_1}(S, f_{\lambda}(S)), f_{\lambda}(S), \gamma) = 0 \tag{44}$$

in order to obtain a bi-elementary path with the maximum possible curvature. Theorem 2 states that a unique solution of (44) can be obtained using the Newton iteration in (29).

Theorem 2. Consider that $S \in [0, 500]$, $0.3 \leq \gamma \leq 1$ and $0 < \Delta Y \leq 10$. Then, the nonlinear equation in (44) has a unique solution S^* that can be computed by the Newton iteration in (29) with the initial value $S_0 = 500$.

The proof of Theorem 2 is provided in Appendix B. We again note that the parameter intervals in Theorem 2 are chosen according to practical considerations. First, the same values for ΔY as in Section 3.2 are assumed. Second, the values for γ are selected based on the fact that smaller values of γ lead to very long bi-elementary paths as was already observed in Fig. 9. In addition, it will be further highlighted in Section 3.4 that small values for γ are not suitable for lane change trajectories. Finally, the maximum value for S is chosen such that the Newton method always finds a solution as is shown in Appendix B.

In summary, this section develops a straightforward procedure for selecting the parameters of a bi-elementary lane change path for a given entry velocity v_0 , maximum acceleration a_{\max} and shape parameter γ . The steps of the procedure are listed as follows.

1. Determine the solution S^* of (44) using the Newton method
2. Compute $\lambda^* = f_\lambda(S^*)$ from (41) and $k_1^* = f_{k_1}(S^*, \lambda^*)$ from (42).
3. Evaluate the desired bi-elementary path as $\mathcal{B}(S^*, k_1^*, \lambda^*, \gamma)$.

The resulting bi-elementary path is the shortest path for a given value of γ that fulfills the curvature constraint in (37) for all possible velocity profiles that start from the entry velocity v_0 and that meet the acceleration constraint a_{\max} . A suitable choice for the parameter γ will be discussed in the subsequent section.

3.4. Trajectory Examples

In this section, we validate the proposed method by several examples. We consider different friction coefficients $\mu = 0.82$ (dry asphalt) and $\mu = 0.5$ (wet asphalt) and accelerations up to 5 m/sec^2 . Considering that accelerations below $a = 2 \text{ m/sec}^2$ are considered as comfortable [32, 9, 19], $a_{\max} = 5 \text{ m/sec}^2$ is selected as a case with a large acceleration.

In the first example, the entry velocity is $v_0 = 20 \text{ m/sec}$, the friction coefficient is $\mu = 0.82$ (which corresponds to dry road) and $\gamma = 1$. Fig. 10 shows the computed bi-elementary path (upper part) and its curvature $k(s)$ with the corresponding maximum curvature $k_{\max}(s)$ (lower part) for different maximum accelerations. It is readily observed that the bi-elementary paths are computed such that the curvature constraint $k_{\max}(s)$ is met. In accordance with (41) and (42), $k(s)$ equals k_{\max} at the two points of maximum curvature such that there is no feasible shorter bi-elementary path. Comparing the different accelerations, it is clear that larger accelerations require a longer arc-length due to the reduced maximum curvature.

Fig. 11 considers the same case as Fig. 10 with the difference that the entry velocity $v_0 = 40 \text{ m/sec}$ is increased. Since a larger entry-velocity implies a reduced maximum curvature in (37), the bi-elementary paths in this case are considerably longer compared to the ones in Fig. 10.

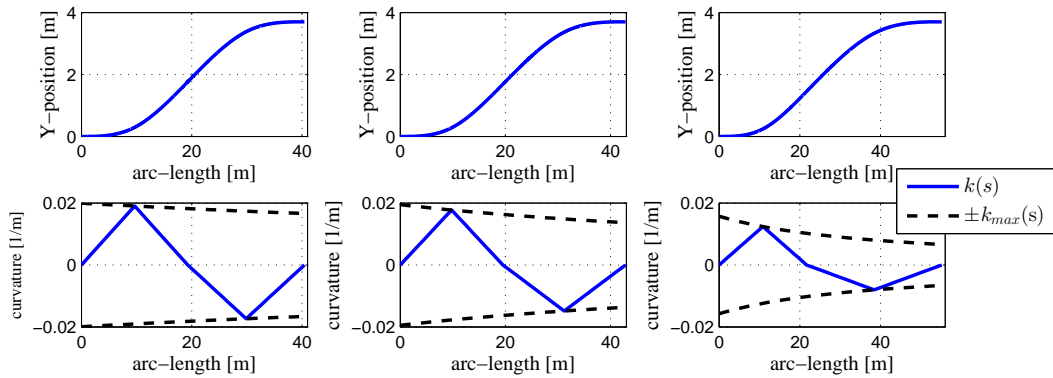


FIGURE 10. Trajectory computation for $v_0 = 20$ m/sec, $\gamma = 1$, $\mu = 0.82$ and $a_{\max} = 1$ m/sec² (left), $a_{\max} = 2$ m/sec² (middle) and $a_{\max} = 5$ m/sec² (right).

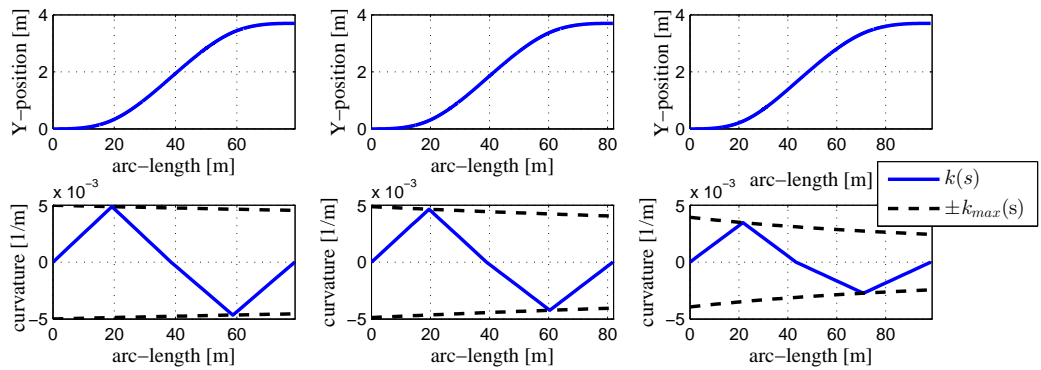


FIGURE 11. Trajectory computation for $v_0 = 40$ m/sec, $\gamma = 1$, $\mu = 0.82$ and $a_{\max} = 1$ m/sec² (left), $a_{\max} = 2$ m/sec² (middle) and $a_{\max} = 5$ m/sec² (right).

Fig. 12 repeats the experiment in Fig. 10 with a reduced friction coefficient $\mu = 0.5$. It can again be seen that the resulting bi-elementary paths perform the lane change with the smallest possible arc-length, whereby the arc-length is increased compared to Fig. 10. In particular, it turns out that an acceleration of $a_{\max} = 5$ m/sec² is not tolerable in this case. Fig. 12 shows the computation for $a = 4$ m/sec² because of this reason.

The previous examples are evaluated for $\gamma = 1$, that is, there is no straight line segment in the resulting bi-elementary paths. We next study the effect of changing γ using $v_0 = 20$ m/sec, $a_{\max} = 2$ m/sec² and $\mu = 0.82$. The resulting bi-elementary paths are shown in Fig. 13. It is clear from this experiment that smaller values of γ lead to longer trajectories. This effect is mainly caused by the usage of a non-zero curvature during a shorter fraction of the overall arc-length when γ is decreased. We note that the same effect was observed for all experiments with different values of v_0 , μ , a_{\max} and ΔY . An analytical evaluation of this observation is not in the scope of this paper.

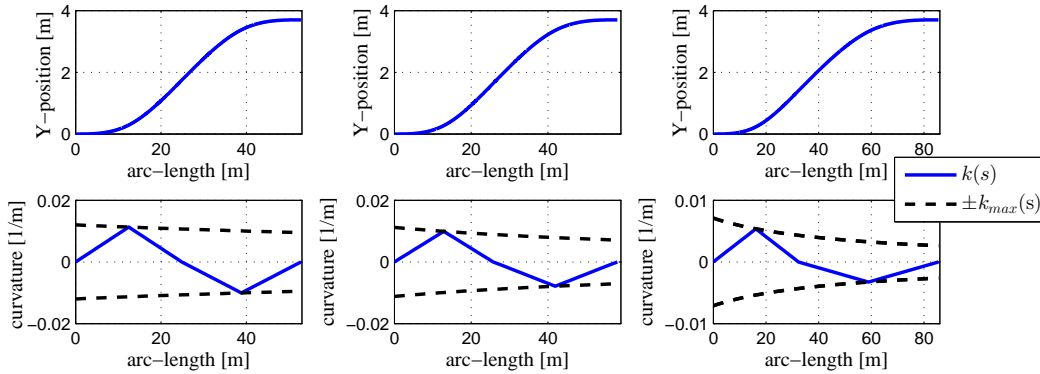


FIGURE 12. Trajectory computation for $v_0 = 20$ m/sec, $\gamma = 1$, $\mu = 0.5$ and $a_{\max} = 1$ m/sec² (left), $a_{\max} = 2$ m/sec² (middle) and $a_{\max} = 4$ m/sec² (right).

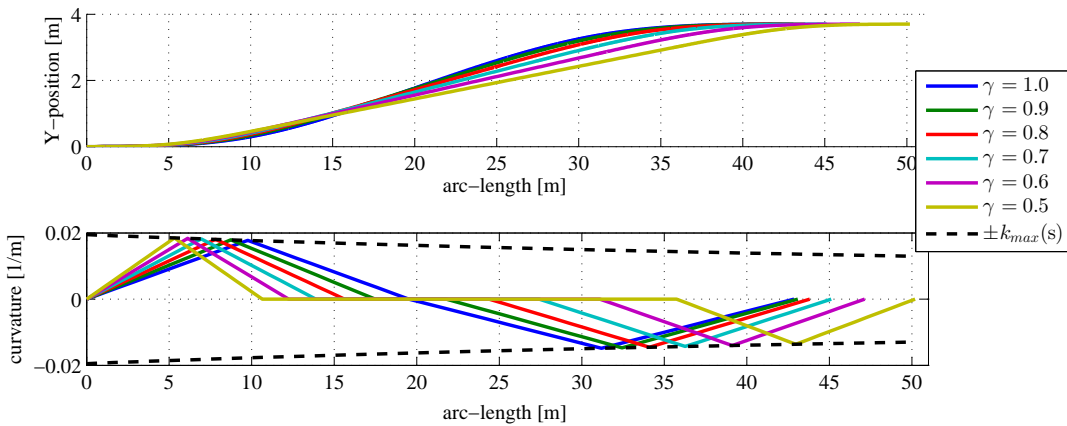


FIGURE 13. Trajectory computation for $v_0 = 20$ m/sec, $\mu = 0.82$ and $a_{\max} = 2$ m/sec² and different values of γ .

In summary, the evaluation in this section shows that the proposed parameter selection method in Section 3.3 indeed determines bi-elementary paths for lane changes with the shortest possible arc-length, while meeting the imposed curvature constraints. Considering that the shortest lane change trajectory was obtained for $\gamma = 1$, it is suggested to apply the proposed method for this value of γ . It is finally pointed out that the proposed parameter selection method can be applied in real-time. It is only required to solve (43), which can be done using the Newton method with a limited number of iterations. In all our experiments, a solution of (43) for $\varepsilon = 10^{-8}$ (which corresponds to a precision of $1 \mu\text{m}$) could be obtained within not more than 15 iterations.

4. Realization and Evaluation

The lane change trajectories in Section 3 were computed based on the maximum curvature evaluation in (37), which is based on a point mass vehicle model. This section validates the suitability of the computed trajectories using the control architecture in Fig. 2 with a nonlinear vehicle model. The model equations are presented in Section 4.1 and simulation results for different velocity profiles and friction coefficients are shown in Section 4.2 and 4.3.

4.1. Vehicle Model

The study in this paper is based on the dynamic bicycle model as shown in Fig. 14. The global coordinates are X, Y and Ψ and a body coordinate frame with the coordinates x, y, ψ is attached to the vehicle center of gravity (CG).

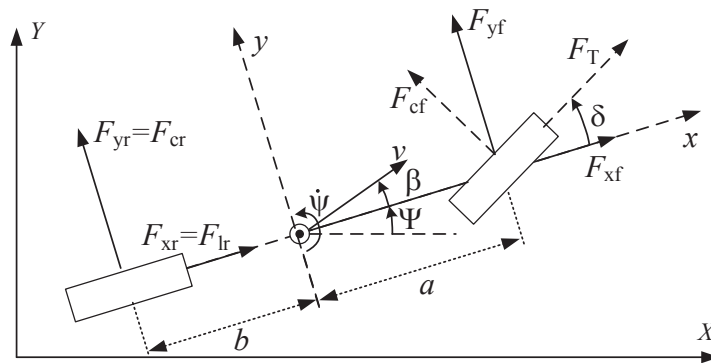


FIGURE 14. Dynamic Bicycle Model

The relation between the inertial and body coordinates is given by

$$\dot{X} = \dot{x} \cos(\Psi) - \dot{y} \sin(\Psi) \tag{45}$$

$$\dot{Y} = \dot{x} \sin(\Psi) + \dot{y} \cos(\Psi) \tag{46}$$

$$\dot{\Psi} = \dot{\psi}. \tag{47}$$

The dynamic equations in the body frame are

$$\ddot{x} = \dot{y} \dot{\psi} + \frac{F_{xf} + F_{xr}}{m} \tag{48}$$

$$\ddot{y} = -\dot{x} \dot{\psi} + \frac{F_{yf} + F_{yr}}{m} \tag{49}$$

$$\ddot{\psi} = \frac{aF_{yf} - bF_{yr}}{I_{zz}} \tag{50}$$

Hereby, m is the vehicle mass, I_{zz} is the moment of inertia and a, b are the distances between the wheels and the CG. The longitudinal forces F_{xf}, F_{xr} and the lateral forces F_{yf}, F_{yr} at the front and

rear tires are computed using (51) to (54) depending on the respective forces in the wheel direction F_T , F_{cf} , F_{lr} and F_{cr} .

$$F_{xf} = F_T \cos(\delta) - F_{cf} \sin(\delta) \text{ (front wheel, x-direction)} \quad (51)$$

$$F_{yf} = F_T \sin(\delta) + F_{cf} \cos(\delta) \text{ (front wheel, y-direction)} \quad (52)$$

$$F_{xr} = F_{lr} = 0 \text{ (rear wheel, x-direction)} \quad (53)$$

$$F_{yr} = F_{cr} \text{ (rear wheel, y-direction)} \quad (54)$$

F_T is the traction force that is provided by the engine and $F_{lr} = 0$ when using actuation at the front tires. The forces F_{cf} and F_{cr} depend on the lateral tire slip angles α_f (front) and α_r (rear) of the respective tire:

$$\alpha_f = \tan^{-1}\left(\frac{\dot{y} + a\dot{\psi}}{\dot{x}}\right) - \delta \quad (55)$$

$$\alpha_r = \tan^{-1}\left(\frac{\dot{y} - b\dot{\psi}}{\dot{x}}\right) \quad (56)$$

Then, the tire forces can be computed using the magic formula [21] that is frequently used in the literature [3, 25, 12]. Its basic form is given in the following equations [22, 21]:

$$F_{cf} = D_{cf} \sin(C_{cf} \tan^{-1}(B_{cf} \alpha_f - E_{cf}(B_{cf} \alpha_f - \tan^{-1}(B_{cf} \alpha_f)))), \quad (57)$$

$$F_{cr} = D_{cr} \sin(C_{cr} \tan^{-1}(B_{cr} \alpha_r - E_{cr}(B_{cr} \alpha_r - \tan^{-1}(B_{cr} \alpha_r))). \quad (58)$$

In this paper, we make the common assumption that the parameters for the rear and front tires are equal. That is, we use B , C , D and E . Here, D determines the maximum possible lateral tire force, which depends on the normal force of the vehicle. Using the vehicle mass m and the road friction coefficient μ , the maximum lateral force is given by

$$D = \mu m g. \quad (59)$$

The remaining parameters are shape parameters that determine the dependency of the tire force on the slip angle. In this paper, we use the parameters from [26] as summarized in Table 1.

TABLE 1. Vehicle parameters.

m	I_{zz}	B	C	D	E	a	b
1480	1950	8.22	1.65	$-1.7 \cdot 10^4$	-10	1.421	1.029

4.2. Lane Change Experiments for Dry Roads

In this section, we consider the case of dry roads such that $\mu = 0.82$. We perform simulation experiments in the control architecture in Fig. 2 using the vehicle model in Section 4.1. Lateral control is realized by the lane keeping method in [15] and the traction force F_T is computed such

that the desired acceleration profile for each experiment is achieved. In each experiment, the vehicle performs a lane change after traveling 50m on a straight road and continues driving on that road after the lane change until the X-position reaches 250 m. The lane width of 3.7 m is chosen if not stated otherwise. Following the discussion in Section 3.4, the value $\gamma = 1$ is used.

In the first experiment, the entry velocity is $v_0 = 20$ m/sec and the maximum acceleration is $a_{\max} = 2$ m/sec². In this case, a trajectory with $\lambda^* = 0.46$, $k_1^* = 0.018$ $S^* = 42.86$ m is computed. Fig. 19 shows the simulation result. In the upper plot, the reference trajectory is compared to the actual vehicle trajectory and the lower plot shows the acceleration bound μg as well as the applied longitudinal acceleration a_{long} and the overall acceleration $\sqrt{a_{\text{long}}^2 + a_{\text{lat}}^2}$. It is readily observed that the vehicle is able to follow the reference trajectory with a small error. This is due to the fact that the reference trajectory is computed respecting the constraint in (37) on the maximum curvature. As a result, the overall acceleration does not exceed the acceleration bound as can be seen in the lower part of Fig. 15.

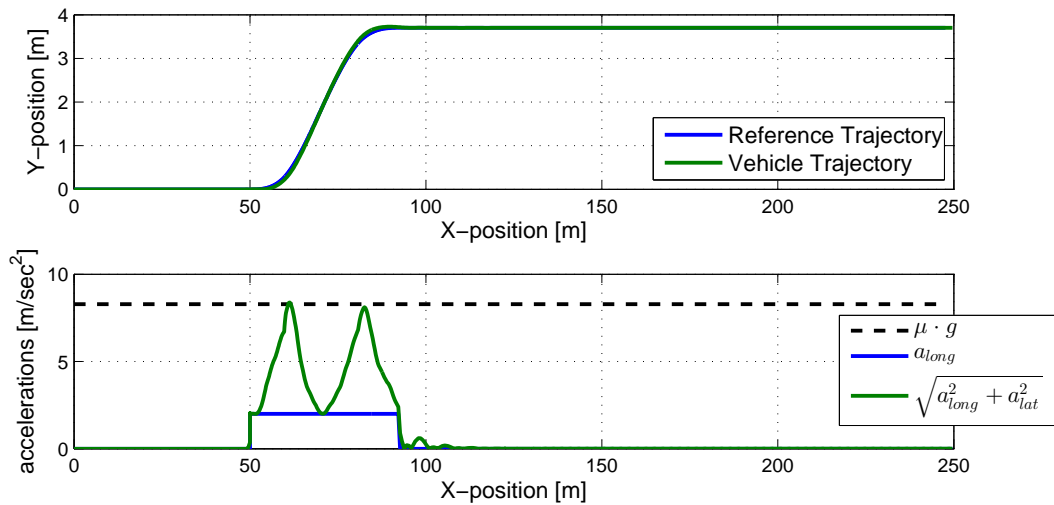


FIGURE 15. Trajectory following for $v_0 = 20$ m/sec, $a_{\max} = 2$ m/sec², $\mu = 0.82$ and $\Delta Y = 3.7$ m.

Fig. 16 shows the simulation result for $v_0 = 20$ m/sec and $a_{\max} = 4$ m/sec². In this case a longer lane change trajectory with $\lambda^* = 0.42$, $k_1^* = 0.015$ and $S^* = 49.74$ is obtained due to the increased maximum acceleration. Again, it is the case that the vehicle can follow the computed reference trajectory.

Similarly, Fig. 17 shows the case of an increased entry velocity $v_0 = 40$ m/sec and $a_{\max} = 2$ m/sec². The resulting parameters are $\lambda^* = 0.48$, $k_1^* = 0.005$ and $S^* = 81.80$. It is again observed that the lateral acceleration stays below the computed maximum acceleration such that the vehicle can follow the reference trajectory.

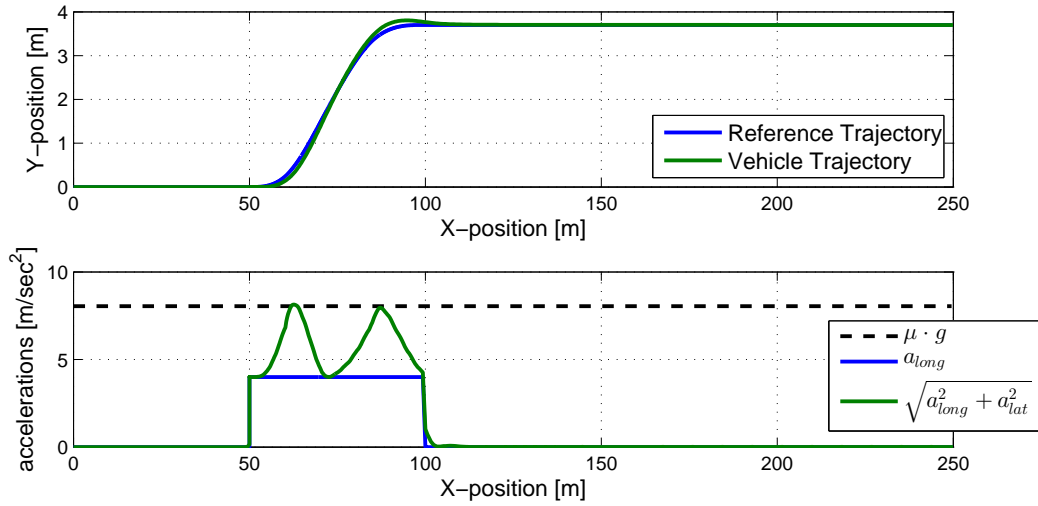


FIGURE 16. Trajectory following for $v_0 = 20$ m/sec, $a_{\max} = 4$ m/sec², $\mu = 0.82$ and $\Delta Y = 3.7$ m.

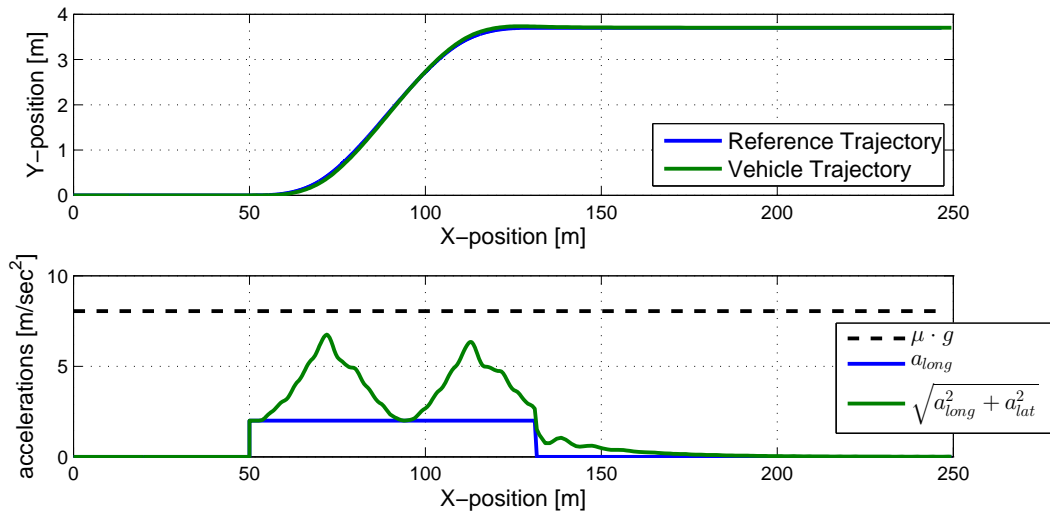


FIGURE 17. Trajectory following for $v_0 = 40$ m/sec, $a_{\max} = 2$ m/sec², $\mu = 0.82$ and $\Delta Y = 3.7$ m.

The last experiment in this section is concerned with the case of a double lane change with $\Delta Y = 7.4$ m at $v_0 = 20$ m/sec and $a_{\max} = 2$ m/sec². The resulting parameter values are $\lambda^* = 0.44$, $k_1^* = 0.017$ and $S^* = 62.94$ m. Fig. 18 shows that the computed reference trajectory is suitable for vehicle following.

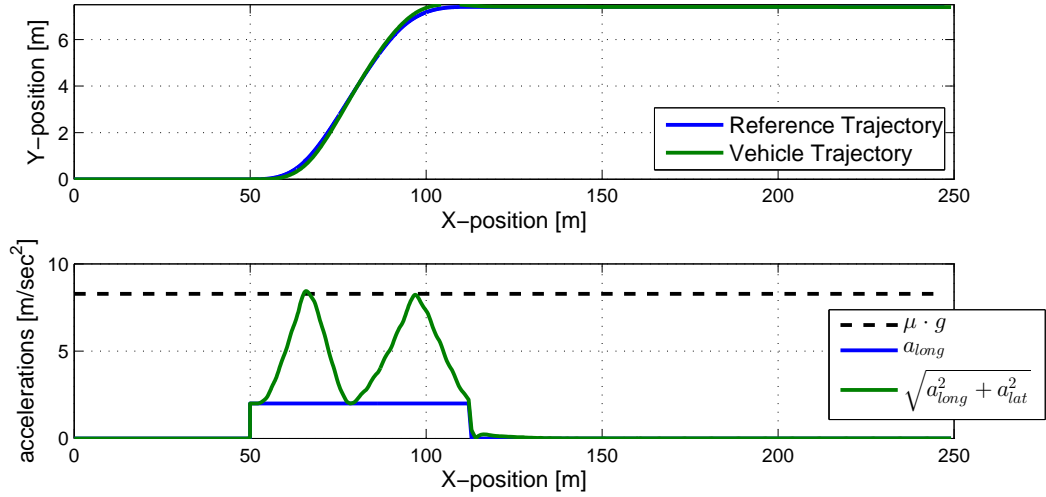


FIGURE 18. Trajectory following for $v_0 = 20$ m/sec, $a_{\max} = 2$ m/sec², $\mu = 0.82$ and $\Delta Y = 7.4$ m.

4.3. Lane Change Experiments for Wet Roads

This section considers the same type of experiment as in the previous section for the case of wet roads. That is, $\mu = 0.5$. Fig. 19 displays the case of $v_0 = 20$ m/sec and $a_{\max} = 2$ m/sec² with the parameter values $\lambda^* = 0.44$, $k_1^* = 0.01$ and $S^* = 58.08$ m. Fig. 20 shows the case of $v_0 = 40$ m/sec and $a_{\max} = 2$ m/sec² with the parameter values $\lambda^* = 0.47$, $k_1^* = 0.003$ and $S^* = 109.47$ m. In comparison to the case of dry roads, it is observed that the computed trajectories are longer. This is expected to the reduced available lateral force. In addition, both figures show that the computed trajectories are suitable for vehicle following and the acceleration bound is always met.

5. Conclusion

The development of self-driving vehicles is an emerging subject both in industry and the recent academic literature. Performing autonomous lane changes is one of the important tasks when realizing self-driving vehicles. In practical applications, it is required to compute vehicle trajectories for lane changes in real-time, while ensuring that the computed trajectories are suitable for the respective driving situation and can be safely followed by vehicles.

The main subject of this paper is the computation of vehicle trajectories for lane changes depending on the driving situation. This paper first points out that a certain type of bi-elementary paths, which is based on clothoid curves, is suitable for performing lane changes. As the first contribution, this paper develops an efficient method for computing the parameters of such bi-elementary path based on a Newton iteration. As the second contribution, this paper determines an analytical

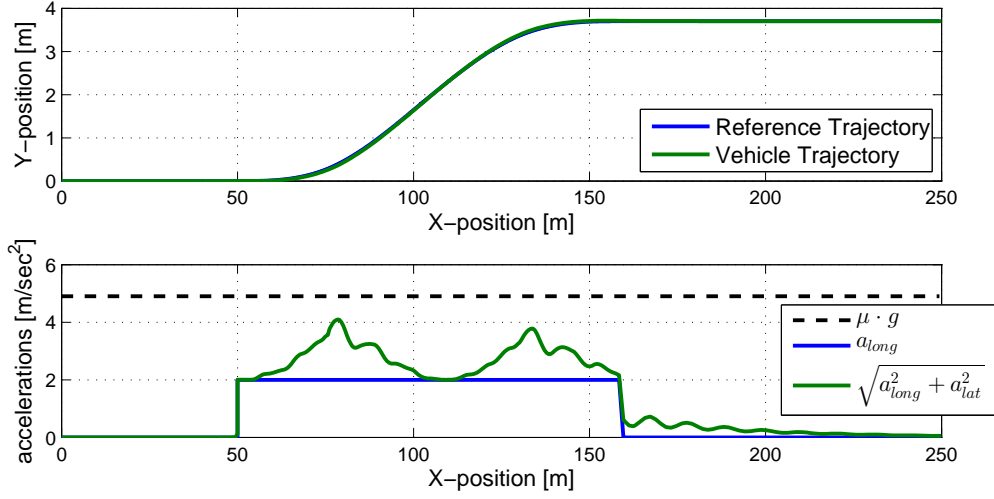


FIGURE 19. Trajectory following for $v_0 = 20$ m/sec, $a_{max} = 2$ m/sec², $\mu = 0.5$ and $\Delta Y = 3.7$ m.

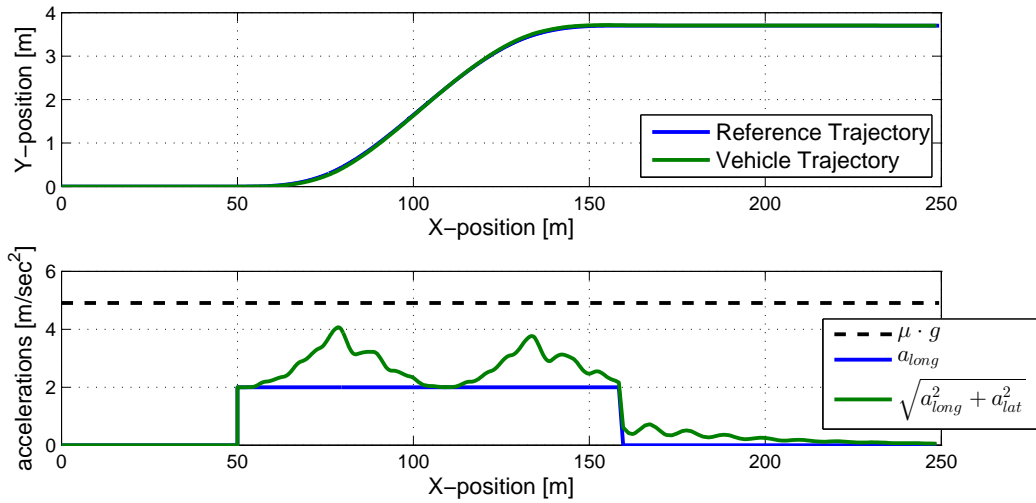


FIGURE 20. Trajectory following for $v_0 = 40$ m/sec, $a_{max} = 2$ m/sec², $\mu = 0.5$ and $\Delta Y = 3.7$ m.

bound on the path curvature depending on the maximum velocity profile of a vehicle during a lane change. Using this bound, this paper proposes a computational procedure for selecting the parameters of bi-elementary paths that are suitable for lane change trajectories. This parameter selection can be efficiently carried out in real-time based on the current vehicle velocity and a bound on the admissible acceleration. Simulation experiments with a nonlinear vehicle model show that the proposed method determines suitable lane change trajectories.

This paper focuses on the case of straight roads. In future work, it is intended to extend the obtained results to the case of curved roads. In addition, the joint computation of an optimal velocity profile and the desired lane change trajectory parameters will be investigated.

Acknowledgments

This work was supported by the Scientific and Technological Research Council of Turkey (TUBITAK) [Award 115E372].

References

- [1] "IEEE news release," http://www.ieee.org/about/news/2012/5september_2_2012.html, 2. September 2012.
- [2] "Autonomous cars – self-driving the new auto industry paradigm," Morgan Stanley Blue Paper, Tech. Rep., November 2013.
- [3] R. Attia, R. Orjuela, and M. Basset, "Coupled longitudinal and lateral control strategy improving lateral stability for autonomous vehicle," in *American Control Conference (ACC), 2012*, June 2012, pp. 6509–6514.
- [4] K. G. Baass, "The use of clothoid templates in highway design," *Transportation Forum*, vol. 1, pp. 47–52, 1984.
- [5] J. L. Buchanan and P. R. Turner, *Numerical Methods and Analysis*. McGraw-Hill, Inc., New York, 1992.
- [6] J. Chen, P. Zhao, T. Mei, and H. Liang, "Lane change path planning based on piecewise bezier curve for autonomous vehicle," in *2013 IEEE International Conference on Vehicular Electronics and Safety (ICVES)*, 2013, pp. 17–22.
- [7] P. J. Davis, *Spirals: from Theodorus to Chaos*. A. K. Peters, Wellesley, Maine, 1993.
- [8] P. Dingle and L. Guzzella, "Optimal emergency maneuvers on highways for passenger vehicles with two- and four-wheel active steering," in *American Control Conference (ACC), 2010*, June 2010, pp. 5374–5381.
- [9] E. Dovgan, T. Tušar, M. Javorski, and B. Filipič, "Discovering comfortable driving strategies using simulation-based multiobjective optimization," *Informatica*, vol. 36, no. 3, pp. 319–326, 2012.
- [10] P. Falcone, M. Tufo, F. Borrelli, J. Asgari, and H. Tsengz, "A linear time varying model predictive control approach to the integrated vehicle dynamics control problem in autonomous systems," in *Decision and Control, 2007 46th IEEE Conference on*, Dec 2007, pp. 2980–2985.
- [11] J. Funke and J. C. Gerdes, "Simple clothoid lane change trajectories for automated vehicles incorporating friction constraints," *ASME. J. Dyn. Sys., Meas., Control*, vol. 138, no. 2, pp. 021 002–021 002–9, 2015.
- [12] M. P. Gianpiero Mastinu, Ed., *Road and Off-Road Vehicle System Dynamics Handbook*. CRC Press, 2014.
- [13] K. Kritayakirana and J. C. Gerdes, "Autonomous vehicle control at the limits of handling," *International Journal of Vehicle Autonomous Systems*, vol. 10, no. 4, pp. 271–296, 2012.
- [14] Z. Li and D. Meek, "Smoothing an arc spline," *Computers & Graphics*, vol. 29, no. 4, pp. 576–587, 2005. [Online]. Available: <http://www.sciencedirect.com/science/article/pii/S0097849305000907>
- [15] R. Marino, S. Scalzi, and M. Netto, "Nested {PID} steering control for lane keeping in autonomous vehicles," *Control Engineering Practice*, vol. 19, no. 12, pp. 1459–1467, 2011.
- [16] B. Mashadi and M. Majidi, "Two-phase optimal path planning of autonomous ground vehicles using pseudo-spectral method," *Proceedings of the Institution of Mechanical Engineers, Part K: Journal of Multi-body Dynamics*, 2014. [Online]. Available: <http://pik.sagepub.com/content/early/2014/06/11/1464419314538245.abstract>

- [17] D. S. Meek and D. J. Walton, "An arc spline approximation to a clothoid," *J. Comput. Appl. Math.*, vol. 170, no. 1, pp. 59–77, Sep. 2004. [Online]. Available: <http://dx.doi.org/10.1016/j.cam.2003.12.038>
- [18] D. Meek and D. Walton, "A note on finding clothoids," *Journal of Computational and Applied Mathematics*, vol. 170, no. 2, pp. 433–453, 2004. [Online]. Available: <http://www.sciencedirect.com/science/article/pii/S0377042704000925>
- [19] A. K. Nandi, D. Chakraborty, and W. Vaz, "Design of a comfortable optimal driving strategy for electric vehicles using multi-objective optimization," *Journal of Power Sources*, vol. 283, pp. 1–18, 2015.
- [20] F. E. P. E. Jahnke, *Tables of Functions with Formulae and Curves*, 4th ed. Dover Publications, New York, 1945.
- [21] H. B. Pacejka, *Tire and Vehicle Dynamics*, 3rd ed. Oxford: Butterworth-Heinemann, 2012.
- [22] H. B. Pacejka and I. J. M. Besselink, "Magic formula tyre model with transient properties," *Vehicle System Dynamics*, vol. 27, no. sup001, pp. 234–249, 1997. [Online]. Available: <http://dx.doi.org/10.1080/00423119708969658>
- [23] R. Pepy, A. Lambert, and H. Mounier, "Path planning using a dynamic vehicle model," in *Information and Communication Technologies, 2006. ICTTA '06. 2nd*, vol. 1, 2006, pp. 781–786.
- [24] G. Rafiq, B. Talha, M. Patzold, J. Gato Luis, G. Ripa, I. Carreras, C. Coviello, S. Marzorati, G. Perez Rodriguez, G. Herrero, and M. Desaegeer, "What's new in intelligent transportation systems?: An overview of european projects and initiatives," *Vehicular Technology Magazine, IEEE*, vol. 8, no. 4, pp. 45–69, Dec 2013.
- [25] A. Rucco, G. Notarstefano, and J. Hauser, "Optimal control based dynamics exploration of a rigid car with longitudinal load transfer," *Control Systems Technology, IEEE Transactions on*, vol. 22, no. 3, pp. 1070–1077, May 2014.
- [26] —, "Optimal control based dynamics exploration of a rigid car with longitudinal load transfer," *Control Systems Technology, IEEE Transactions on*, vol. 22, no. 3, pp. 1070–1077, May 2014.
- [27] A. Schindler, G. Maier, and S. Pangerl, "Exploiting arc splines for digital maps," in *2011 14th International IEEE Conference on Intelligent Transportation Systems (ITSC)*, Oct 2011, pp. 1–6.
- [28] T. S. L. Sumit Ghosh, *Intelligent Transportation Systems: Smart and Green Infrastructure Design*. CRC Press, 2010.
- [29] J. S. Sussman, *Perspectives on Intelligent Transportation Systems (ITS)*, 1st ed. Springer US, 2005.
- [30] P. Varaiya, "Smart cars on smart roads: problems of control," *Automatic Control, IEEE Transactions on*, vol. 38, no. 2, pp. 195–207, Feb 1993.
- [31] M. Werling, S. Kammel, J. Ziegler, and L. Gröll, "Optimal trajectories for time-critical street scenarios using discretized terminal manifolds," *The International Journal of Robotics Research*, vol. 31, no. 3, pp. 346–359, 2012. [Online]. Available: <http://ijr.sagepub.com/content/31/3/346.abstract>
- [32] Z. Wu, Y. Liu, and G. Pan, "Smart car control model for brake comfort based on car following," *IEEE Transactions on Intelligent Transportation Systems*, vol. 10, no. 1, pp. 42–46, 2009.
- [33] H. Yoshida, S. Shinohara, and M. Nagai, "Lane change steering manoeuvre using model predictive control theory," *Vehicle System Dynamics*, vol. 46, no. sup1, pp. 669–681, 2008. [Online]. Available: <http://dx.doi.org/10.1080/00423110802033072>

Appendix A. Proof of Theorem 1

We first state an existing result regarding the convergence of the Newton method from [5].

Proposition 3. Consider a function $f : z \mapsto f(z) : [a, b] \rightarrow \mathbb{R}$. Assume that $f(z)$ is twice differentiable and satisfies the following conditions on $[a, b]$:

1. $f(a) < 0$ and $f(b) > 0$
2. $f'(z) > 0$ on $[a, b]$
3. $f''(z) > 0$ on $[a, b]$

Then, the Newton iteration converges to a unique solution z^* of the equation $f(z) = 0$ in $[a, b]$ if the starting value fulfills $z_0 \geq z^*$.

In order to prove Theorem 1 we show that (28) fulfills the conditions in Proposition 3. We consider the function $f(\alpha) = f_1(\alpha)$ in (28) and write

$$f_1(\alpha) = g_1(\alpha, \gamma) - \Delta Y \lambda \gamma k_1$$

with

$$g_1(\alpha, \gamma) = 2\alpha (\gamma \hat{D}(\alpha) \sin(\alpha/2) + (1 - \gamma) \sin(\alpha)).$$

That is, $g_1(\alpha, \gamma)$ depends on α, γ and $g_1(0, \gamma) = 0$ such that the offset value $f_1(0) = -\Delta Y \lambda \gamma k_1$ is only determined by $\Delta Y, \lambda, \gamma$ and k_1 . The evaluation of $g_1(\alpha, \gamma)$ for values of $\gamma \in (0, 1]$ and the relevant range of $\alpha \in [0, \pi/4]$ is given in Fig. 21.

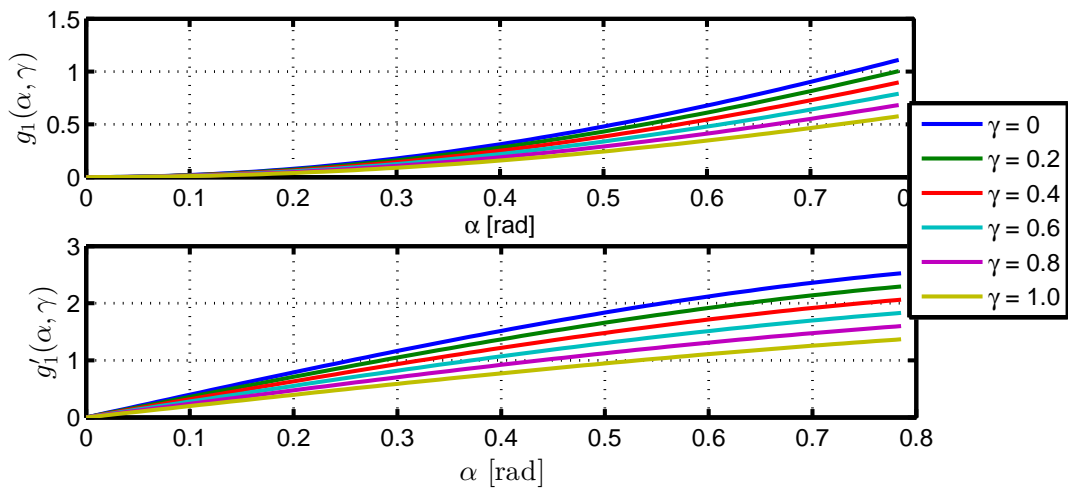


FIGURE 21. $g_1(\alpha, \gamma)$ and $g_1'(\alpha, \gamma)$ for $\gamma \in (0, 1]$ and $\alpha \in [0, \pi/4]$.

Focusing on the interval $[a, b] = [0, \pi/4]$, it is readily observed that $g_1(a, \gamma) = g_1(0, \gamma) = 0$ for all $\gamma \in (0, 1]$ and $g_1(b) = g_1(\pi/4) \geq 0.577$. In order to apply Proposition 3 1), it must hold that $f_1(a) < 0$ and $f_1(b) > 0$. Considering that $f_1(\alpha) = g_1(\alpha, \gamma) - \Delta Y \lambda \gamma k_1$ and $\Delta Y > 0, \lambda > 0, \gamma > 0, k_1 > 0$, it is clear that

$$f_1(a) = f_1(0) = g_1(0, \gamma) - \Delta Y \lambda \gamma k_1 = -\Delta Y \lambda \gamma k_1 < 0.$$

Then, it must be confirmed that $f_1(b) = f_1(\pi/4) = g_1(\pi/4, \gamma) - \Delta Y \lambda \gamma k_1 > 0$. To this end, we determine the largest value of $\Delta Y \lambda \gamma k_1$. It holds by assumption that $\lambda \in (0, 1), \gamma \in (0, 1], 0 \leq k_1 \leq$

0.05 and $\Delta Y \leq 10$. Together, the desired bound evaluates to

$$\Delta Y \lambda \gamma k_1 < 10 \cdot 1 \cdot 0.05 = 0.5 < \min_{\gamma} g_1(b, \gamma) = 0.577.$$

That is, indeed $f_1(b) > 0$ such that condition 1) in Proposition 3 is fulfilled.

In addition, it holds that

$$f_1'(\alpha) = g_1'(\alpha, \gamma) > 0$$

for all values of $\gamma \in (0, 1]$, $\lambda \in (0, 1)$, ΔY and k_1 and $f_1''(\alpha) = g_1''(\alpha, \gamma)$ is always positive for $\alpha \in [0, \pi/4]$ as can be verified by Fig. 21. Hence, condition 2) and 3) in Proposition 3 are also true.

Since it is assumed that only angles in the interval $[0, \pi/4]$ are suitable for lane changes, it suffices to choose $\alpha_0 = \pi/4$ in order to fulfill all conditions in Proposition 3.

Appendix B. Proof of Theorem 2

In order to prove Theorem 2 we show that (44) fulfills the conditions in Proposition 3. For each value of γ , we consider the function $f(S) = f_S(S, \gamma)$ in (44). Inspecting (43), it holds that $f_S(S, \gamma)$ can be written as

$$f_S(S, \gamma) = g_S(S, \gamma) - \Delta Y.$$

The function $g_S(S, \gamma)$ is shown for different values of γ , a_{\max} , v_0 and μ in Fig. 22.

Focusing on the interval $[a, b] = [0, 500]$ for S , it is readily observed that $g_S(a, \gamma) = g_S(0, \gamma) = 0$ for all $\gamma \in [0.3, 1]$ and $g_S(b) = g_1(500) \geq 10.32$. In order to apply Proposition 3 1), it must hold that $f_S(a, \gamma) < 0$ and $f_S(b, \gamma) > 0$. Considering that $f_S(S, \gamma) = g_S(S, \gamma) - \Delta Y$ and $\Delta Y > 0$, it is clear that

$$f_S(a, \gamma) = f_S(0, \gamma) = g_S(0, \gamma) - \Delta Y = -\Delta Y < 0.$$

Similarly, it is confirmed that

$$f_S(b, \gamma) = f_S(500, \gamma) = g_S(500, \gamma) - \Delta Y > 10.32 - 10 > 0.$$

Hence, condition 1) in Proposition 3 is fulfilled.

In addition, it holds that

$$f_S'(S, \gamma) = g_S'(S, \gamma) > 0$$

for all values of $\gamma \in [0.3, 1]$ and $f_S''(S, \gamma) = g_S''(S, \gamma)$ is always positive for $S \in [0, 500]$ as can be verified by Fig. 22. Hence, condition 2) and 3) in Proposition 3 are also true.

Since it is assumed that only arc-lengths in the interval $[0, 500]$ are suitable for lane changes, it suffices to choose $S_0 = 500$ in order to fulfill all conditions in Proposition 3.

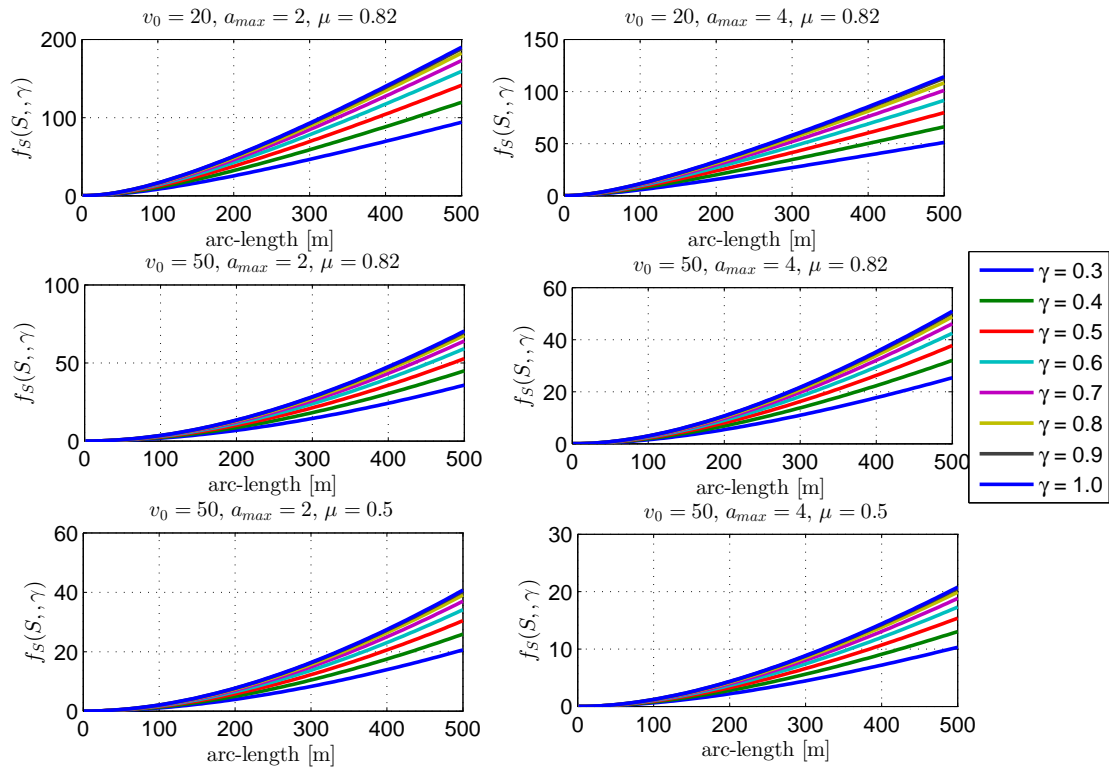


FIGURE 22. Evaluation of f_S in (44) for different values of γ .